Progress In Electromagnetics Research C, Vol. 120, 105–117, 2022

Wideband Diversity MIMO Antenna Design with Hexagonal Slots for 5G Smart Mobile Terminals

Hatim S. Alhaqbani[1], Mohammed M. Bait-Suwailam[2], Maged A. Aldhaeebi[3], and Thamer S. Almoneef[1, *]

Abstract—In this paper, we propose a wideband polarization diversity multiple-input multiple-output (MIMO) antenna array for 5G smart mobile devices. The proposed MIMO antenna array consists of 8-ports dual-polarized L-shaped lines that highly excite radiating slots, where the elements are placed at four-corners of a compact mobile unit of size $75 \times 150\,\text{mm}^2$. The uniqueness of the proposed MIMO antenna structure comes from the deployment of octagon-shaped resonant slots within the metallic ground plane, i.e., the octagonal-slots are etched from the bottom (ground) layer of the main mobile board. Due to the unique slots in the ground plane, wideband impedance has been achieved (3.38–3.8 GHz at −6-dB threshold). The proposed smart phone 8×8 diversity MIMO antenna is designed to support the spectrum of commercial sub-6 GHz 5G communications and cover the frequency range of around 3.5 GHz band with high decoupling between antenna ports. The proposed array is designed, numerically simulated, fabricated, and tested. Good agreement between simulated and measured results was achieved. The MIMO antenna has a satisfactory far-field performance along with very low envelope correlation coefficient (ECC) < 0.055, high diversity of more than 9.95, and very low specific absorption rate ($< 1\,\text{W/kg}$ for a 10-g human tissue).

1. INTRODUCTION

Multiple-input multiple-output (MIMO) technology is considered as a critical part for efficient wireless connectivity in the fifth-generation (5G) mobile communications, which relies on the reliable design of massive-MIMO antenna system with wide coverage in both sub-6 GHz and mm-wave bands as well as integration of smart beamforming techniques. Over the past ten years, there has been renewed research interest from both academia and industry in the design and deployment of MIMO antenna systems for 4G, 5G, and future generation of mobile communications, due to its great impact on reliability, higher transmission rate, and wireless link capacity [1, 2]. Due to the deployment of multi-antenna elements within MIMO technology, one can expect an enhancement to the wireless system reliability, quality of service, and capacity using the multi-path data transmission and reception with a number of available diversity mechanisms. The design of MIMO antenna has been extensively studied and already been implemented in 4G base station and user equipment alike. However, more excitement has been witnessed in the deployment of MIMO technology in 5G smart mobile units [1, 3–9]. In principle, MIMO physical package consists of two or four antenna elements that are distributed according to the aimed diversity mechanism, while a massive MIMO system has a large number of antenna elements that could go over 100 antenna elements [10]. MIMO antenna technology is expected to provide high gain, low bit error rates, and high data capacity as compared against single-input single-output (SISO) antenna

Received 16 March 2022, Accepted 29 April 2022, Scheduled 9 May 2022

* Corresponding author: Thamer S. Almoneef (t.almoneef@psau.edu.sa).

[1] Electrical Engineering Department, College of Engineering, Prince Sattam Bin Abdulaziz University, Al-Kharj 11942, Saudi Arabia. [2] Department of Electrical and Computer Engineering, Sultan Qaboos University, Muscat, Oman. [3] Department of Electronics and Communication Engineering, Hadhramout University, Mukalla, P. O. Box 50512, Yemen.

system. Moreover, as the number of antenna elements is increased, the MIMO antenna system has a great capability to enhance transmission path, resist electromagnetic interference, and scan blindness problems, especially when antenna elements are highly decoupled [1, 11–14].

Due to the expected increase in user equipment within the next couple of years, there has always been a great demand to include large number of antenna elements that need to keep both productivity and entertainment of users to the best experience in terms of quality of service, wireless connectivity, needed bandwidth, and reliability. The design challenges that researchers are facing are: 1) the deployment of a large number of multi-antennas within a small footprint area in a mobile handset, 2) ensure minimal electromagnetic interference (mutual coupling) between the antenna elements in such a compact design, and 3) robustness of the MIMO antenna system in terms of near- and far-field and MIMO metrics when it is placed in close-proximity to human tissues.

Various MIMO antenna designs for 4G long-term evolution (LTE) smart mobile applications have already been proposed in the literature [15–19]. The basic deployment of a MIMO antenna system is of course the use of 2×2 multi-antenna elements. More design challenges are expected as the number of antenna elements is increased due to the aforementioned design requirements. Currently, there are different MIMO antenna structures targeting the 5G systems [20–27]. Some of them have focused on the design of multi-antennas for operation within the LTE band 42 (3400–3600 MHz) or LTE band 43 (3600–3800 MHz) [21], and some have targeted the mm-wave bands (28 GHz/38 GHz) [28], while others have proposed designs of multi-antenna elements to cover both bands simultaneously [29–31]. Among the main design issues in some of the earlier proposed prototypes are their narrow operational bandwidth, insufficient decoupling between antenna elements, and relatively large space area used within the user equipment main board. As for 5G mobile users in next and future mobile handset generations, there should be an adequate wide operating bandwidth, compactness in the design, and of course high isolation among MIMO multi-antenna elements.

In this work, we present an efficient design of a dual-polarized wideband MIMO antenna system targeting 5G smart mobile handsets. We first present the design of a single (two elements) antenna unit based on a newly developed octagon-shaped resonant slot. Further, we present the design and layout of an 8×8 MIMO antenna array within a mobile handset. Numerical full-wave simulations are carried out here using the time-domain solver of the computer simulation technology (CST) software. Moreover, we present numerical results and validate with measured data. The results are discussed, and MIMO performance metrics are assessed for the proposed wideband diversity MIMO antenna structure, including radiation patterns, gain, efficiency, diversity gain, and envelope correlation coefficient.

2. THE PROPOSED DUAL-POLARIZED 5G MIMO ANTENNA SYSTEM

2.1. Two-Element with an Octagon Slot

The single (two) antenna structure has been designed and numerically simulated in order to function well within the 5G wireless communications covering the 3.5 GHz band. In order to achieve diversity, a dual-polarized antenna structure is considered in this work. The single antenna structure consists of a resonant hexagonal (octagon) slot antenna that is excited using two orthogonal microstrip lines with two identical ports having a 50-Ω impedance. The antenna has a host dielectric substrate (Rogers RO4003C laminate with a dielectric constant, ϵ_r, of 3.38, $\tan\delta = 0.0027$, and thickness of 1.524 mm) with dimensions of $24 \times 24\,\text{mm}^2$, as shown in Figs. 1(a)–(b), where both top and bottom views are illustrated, respectively. Within the numerical simulations, a pair of 50-Ω discrete lumped ports were used to excite the dual-polarized antenna structure. Moreover, metallic layers have been considered as lossy copper with a thickness of 35 µm. The single antenna structure has been optimized carefully in order to operate within the 3.5 GHz-band. All dimensions of the proposed single antenna unit are presented in Table 1.

The above configuration contains a pair of orthogonal L-shaped microstrip feed lines and an octagon slot etched from the metallic ground layer with compact size, making it suitable for next-generation smart phone handsets. The main advantages of this structure are compactness, light weight, and can be integrated easily with radio frequency circuits.

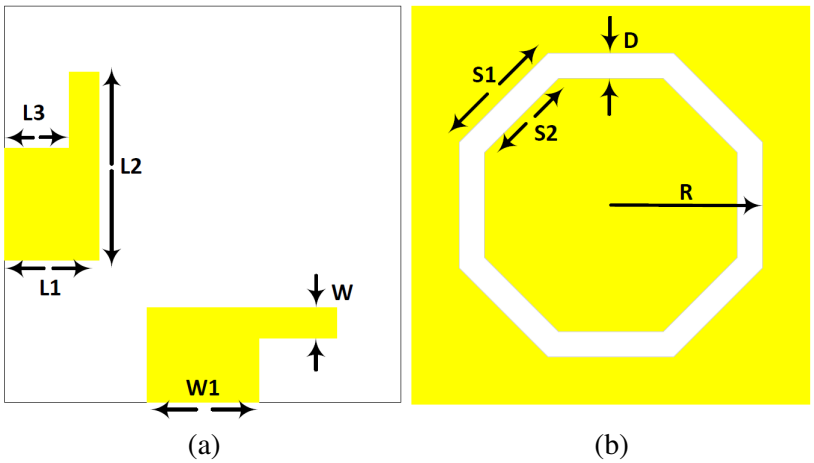

Figure 1. Views of the proposed single antenna element with Octagon slot. (a) Top view and (b) bottom view. Note that yellow area represents metallization.

Table 1. Dimensions of the optimized hexagonal antenna structure.

Parameter (s)	Dimension (in mm)
X	75
Y	150
$W1$	5.5
W	2.3
$L1$	5
$L2$	10.2
$L3$	2.7
R	10
$S1$	7.5
$S2$	7.33
D	0.203

2.2. Proposed MIMO Antenna Design

In this part, we extend our study to an 8-port dual-polarized MIMO antenna array based on the introduced single antenna unit (two-elements). The antenna array contains four elements, each fed by dual-polarized two ports. Thus, we have an eight L-shaped microstrip lines orthogonally placed to achieve diversity and four octagon resonant slots in the metallic ground plane. We have considered realistic dimension of today's 5G smart mobile phones, where a board size of $75 \times 150\,\text{mm}^2$ was used. The simulated design layout of the mobile-phone MIMO antenna array is shown in Figs. 2(a) and (b). Note that the four L-shaped elements are placed at corners having octagon radiating slots on mobile phone PCB. The proposed antenna structure is more compact and has enough space for other antennas and packages, thus making it suitable for the next-generation smart mobile handsets. It has been observed that this compact structure has wide bandwidth and better near-field performance in terms of S-parameters at resonance frequency (both matching and decoupling mechanisms). The observed mutual coupling is very low for the particular bandwidth of interest, where antenna operation within the 5G bandwidth is directly affected by the L-shaped size.

Figure 2(a) depicts a top view of the antenna array with 8 L-shaped transmission lines. In the

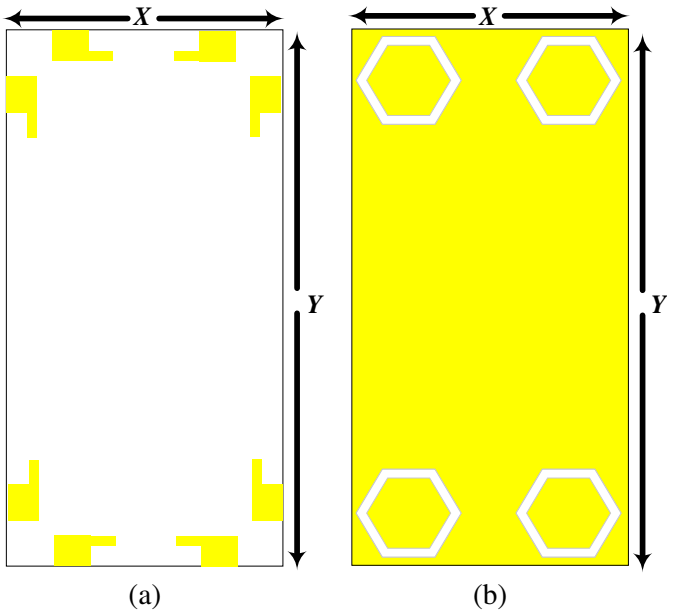

Figure 2. Views of the proposed MIMO antenna structure. (a) Top view and (b) bottom view. Note that yellow area represents metallization.

bottom layer, four octagon-shaped slots are etched out from the metallic layer forming a ground plane for the antenna (see Fig. 2(b)). Numerical simulation results will be presented next, where all materials properties and a sufficiently large open space were ensured within the numerical models.

3. SIMULATION RESULTS

We first present the numerical simulation results from the two-antenna elements unit (dual-polarized), then we show the results in details for the complete 8-port MIMO antenna structure.

3.1. Dual-Polarized Single Antenna Element

The near-field results for the dual-polarized single antenna unit are presented first. The simulated reflection coefficient, S_{11}, of the single antenna element is shown in Fig. 3. As shown from Fig. 3,

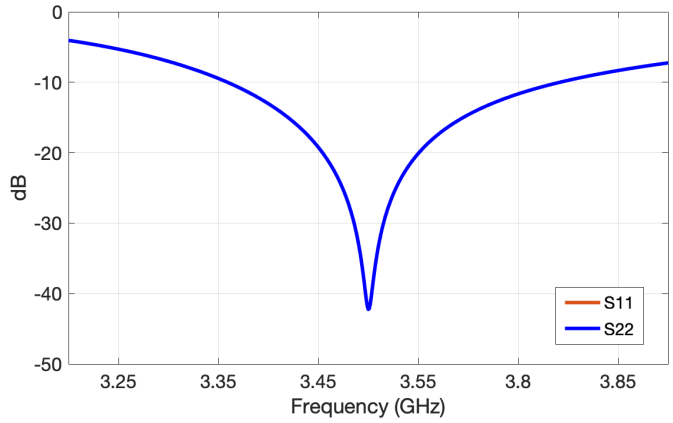

Figure 3. Simulated reflection coefficient at ports 1 and 2 of the designed dual-polarized antenna structure working at the 3.5 GHz band.

wideband impedance matching is achieved from ports 1 and 2, simultaneously, covering the frequency band of 3.5 GHz. Thus, it fits very well with the 5G smart mobile phone units communications. A very sharp dip for S_{11} is observed at 3.5 GHz with around −43 dB, indicating a high resonance at the frequency of interest.

Since two-ports are used for feeding the multi-antenna elements, it is important to investigate both matching from both ports as well as the mutual coupling between the two ports, S_{21}. The simulation results for both S_{11} and S_{21} are shown in Fig. 4(a). Good matching for both ports was achieved, over a wide impedance bandwidth from 3.3 GHz to 3.9 GHz (at −6 dB level) covering the 5G-band (3.3–3.9 GHz), while at the same time maintaining a very low mutual coupling between the two ports ($|S_{21}| < -15$ dB). Thus, this will insure low cross-correlation between the two ports, hence it is expected to achieve a better envelope correlation. Fig. 4(b) depicts the surface electric field strength distribution within the metallic (bottom) layer of the mobile board when port 1 was excited. As can be seen, significant field is attained within the hexagonal defected resonator, while at the same time very minimal coupling is seen between ports 1 and 2, due to the deployed polarization diversity.

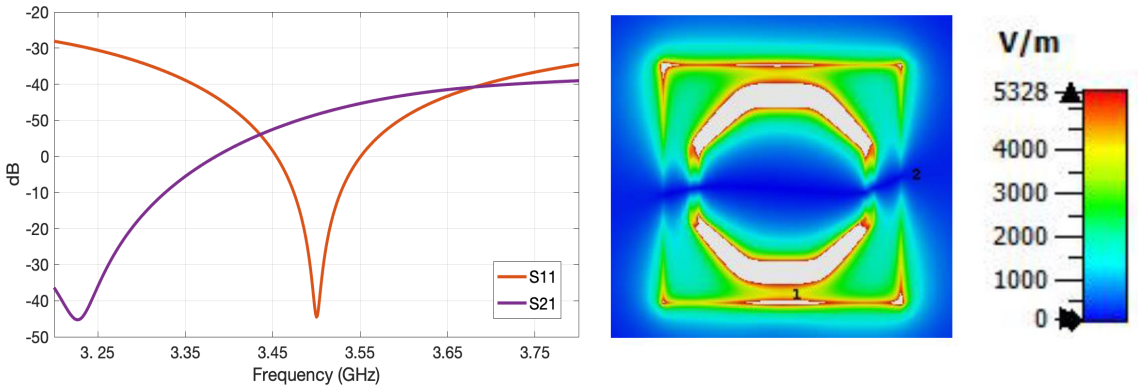

Figure 4. (a) Simulated S_{11} and S_{21} for the proposed single antenna element, and (b) simulated surface E-field strength distribution at the bottom metallic layer of the mobile handset.

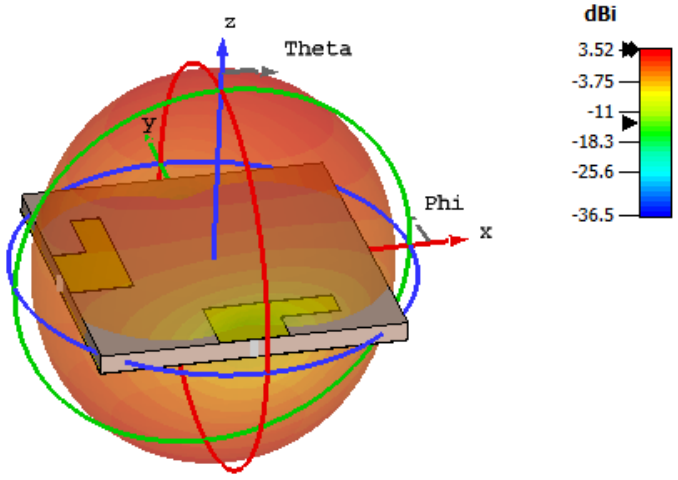

Figure 5. Simulated 3D pattern of the proposed single dual-polarized antenna element at 3.5 GHz.

Figure 5 depicts the 3D radiation pattern of the single antenna unit where maximum radiation in axial direction is maintained, while there was also a minimal radiation in the $\theta = 180°$, due to the perforations from the octagon-shaped resonant slots. Nevertheless, the back-side radiation can also be

alleviated with the use of a slightly larger metallic ground surface to reflect back all the transmitted radiations. Further, a fairly full coverage within the azimuthal plane ($\theta = 180°$) is preserved, which is essential to maintaining reliable coverage for the mobile unit. A maximum gain was achieved around 3.52 dB at the frequency of 3.5 GHz.

3.2. Proposed MIMO Antenna Array

As shown in Fig. 2(a), four dual-polarized identical antenna elements, identical to the designed two-antenna element unit (shown in Fig. 1(a)), were placed at four corners of a modeled smart mobile phone, thus comprising an 8-port MIMO antenna system. The proposed MIMO antenna array was numerically simulated, where good performance from both reflection coefficient and mutual coupling was achieved within the frequency band of interest. The simulated reflection coefficient from the first four ports within one side of the modeled mobile device can be seen in Fig. 6. Good impedance matching was achieved for all antenna ports, with a −10-dB matching from 3.48 GHz to 3.7 GHz, while its bandwidth for the −6-dB (common practical threshold level) ranged from 3.38 GHz–3.8 GHz, which covers both the LTE 42 and 43 bands. The effect of mutual coupling among the four ports was also investigated, and simulation results are presented in Fig. 7. A relatively high decoupling between the MIMO antenna ports was achieved, almost below −15 dB over the 3.5 GHz band. This is also demonstrated in Fig. 4(b) and Fig. 8 when port 1 is excited, where very minimal coupling takes place between port 1 and its nearboring ports, i.e., nulls of E-field strength within the hexagonal slot.

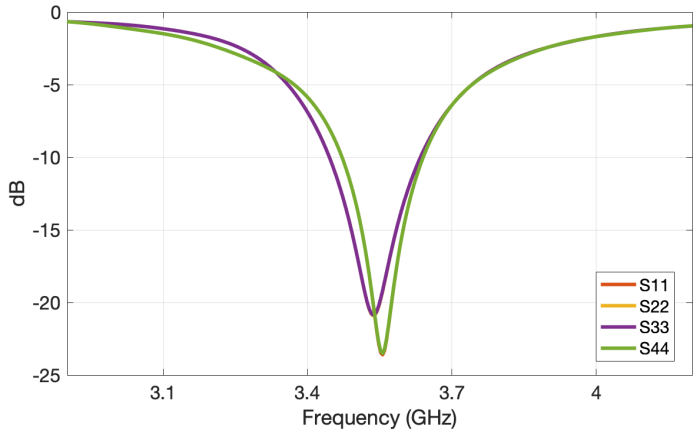

Figure 6. Simulated reflection coefficient for the first four-ports of the proposed MIMO antenna.

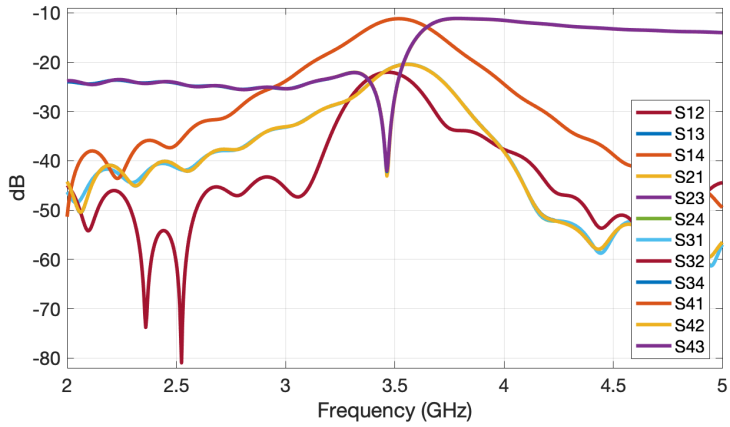

Figure 7. Simulated mutual coupling between the first four-ports of the proposed MIMO antenna.

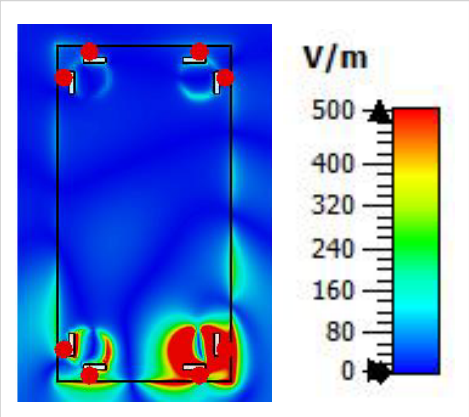

Figure 8. Simulated E-field distribution when port 1 was excited for the proposed MIMO antenna structure.

The 3D far field pattern of the proposed MIMO antenna array is shown in Fig. 9. Good radiation coverage can be seen from the four corners of the modeled mobile unit and can be efficiently used for 5G mobile applications. The simulated peak gain is 4.54 dB at the frequency of 3.5 GHz. The obtained radiation efficiency of this array is 96%, while the total efficiency is 93.6%.

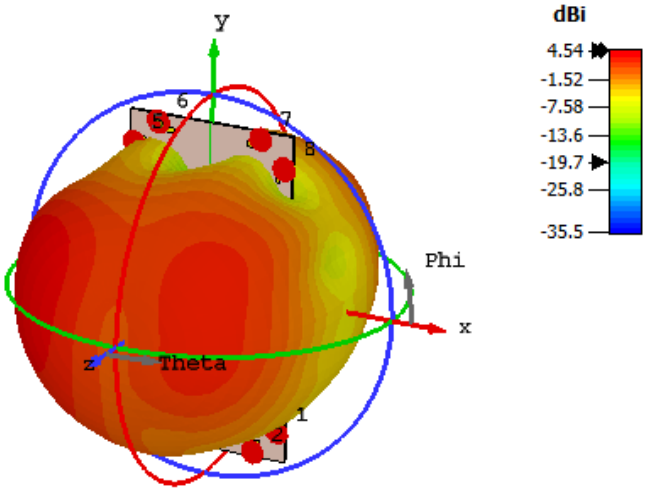

Figure 9. Simulated E-field distribution when port 1 was excited for the proposed MIMO antenna structure.

The envelope correlation, also designated as ECC, was numerically computed and is depicted in Fig. 10. The MIMO antenna array in this work has achieved a very low envelope correlation effect over a wideband frequency. It is instructive to highlight here that the ECC was calculated as a post-processing task using the following relation [32]

$$\mathrm{ECC} = \frac{|S_{mm}S_{mn} + S_{mn}S_{nm}|}{\left(1 - |S_{mn}|^2 - |S_{nm}|^2\right)\left(1 - |S_{nm}|^2 - |S_{nn}|^2\right)}, \tag{1}$$

where S_{mm} is related to the reflection coefficient at port m, while S_{mn} is related to the cross coupling between ports m and n.

Figure 11(a) shows the total efficiency of the MIMO antenna array. It is observed that the array has a satisfactory efficiency within the 3.3 GHz to 3.6 GHz band. Another MIMO performance metric is the

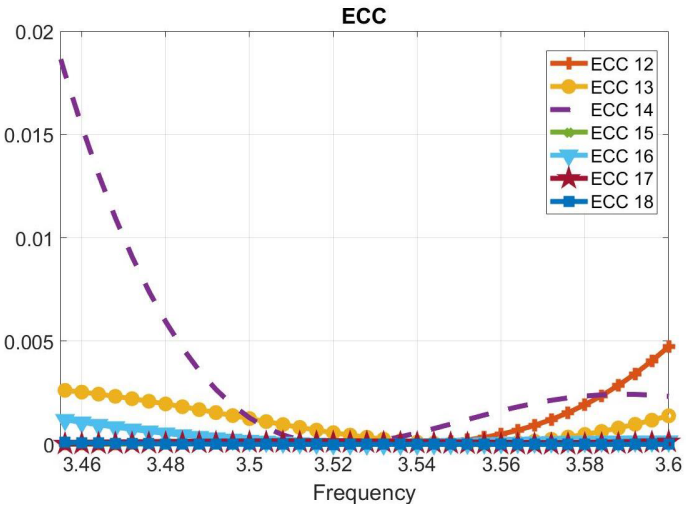

Figure 10. Simulated ECC of the proposed MIMO antenna array where the labeling of each curve (ECC mn) refers to the cross coupling between port m and n.

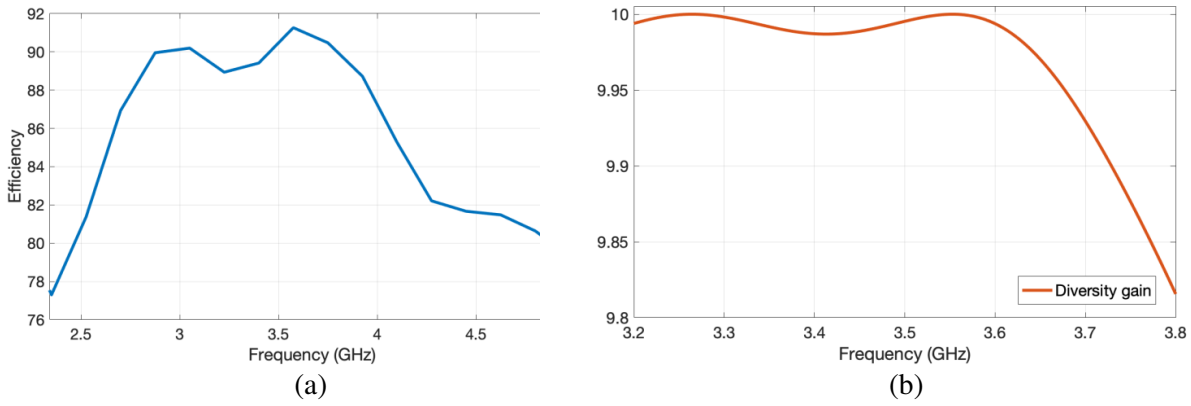

Figure 11. (a) Simulated total efficiency and (b) diversity gain of the proposed MIMO antenna system.

diversity gain, which is related to the amount of transmitted power that could get reduced upon applying a particular diversity mechanism. Fig. 11(b) depicts the diversity gain of the proposed 8×8 MIMO antenna. A high diversity gain was maintained over the 3.5 GHz-band, which shows the robustness of the proposed MIMO antenna in mobile handsets.

4. FABRICATION AND MEASUREMENT RESULTS

The designed MIMO antenna structure was fabricated, and its near field performance was tested, as shown in Figs. 12(a) and (b). An 8.5 GHz 4-port ZNB Rohde and Schwarz Vector Network Analyzer (VNA) was first calibrated, and then the S-parameters of the fabricated MIMO antenna prototype were measured. The eight SMA connectors are shown at the four antenna corner sides (see Fig. 12(b)), while the four octagon slots are etched out of the ground plane as shown in Fig. 12(a).

Figure 13(a) depicts the vector network analyzer, where the fabricated MIMO antenna was connected to the VNA. Fig. 13(b) shows the SMA connectors connected to the antenna array ports. In terms of matching, wideband impedance matching was achieved from the measurements (see Fig. 14(a), which closely match with simulation results of Fig. 6. We highlight here that the first four antenna ports were directly connected to the four-port VNA, while the other four ports were terminated with a matched 50 Ω impedance. Furthermore, the S-parameters of mutual-coupling between MIMO antenna

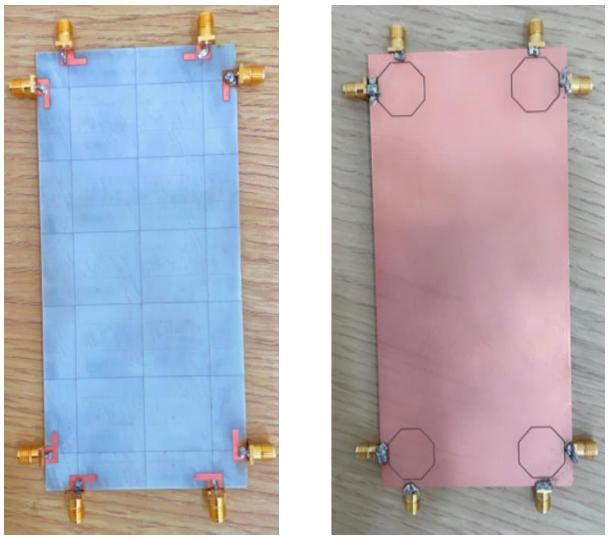

(a) (b)

Figure 12. (a) Top view of the fabricated antenna array and (b) bottom view of the fabricated antenna array showing the octagon slots etched from the metallic ground plane.

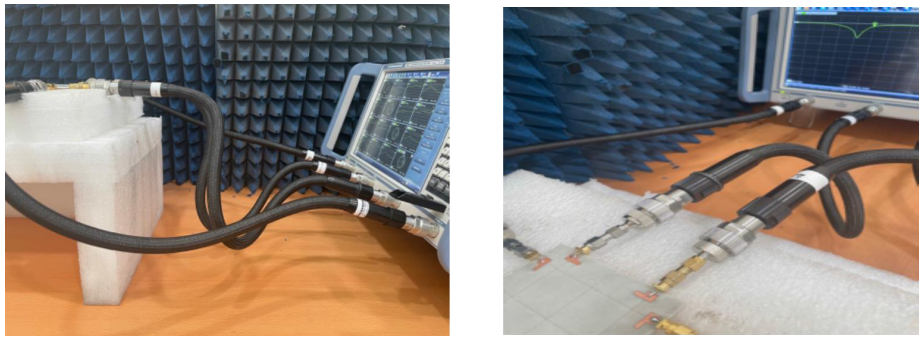

(a) (b)

Figure 13. (a) Side and (b) lateral views showing the fabrication setup with the VNA connections to the proposed MIMO antenna.

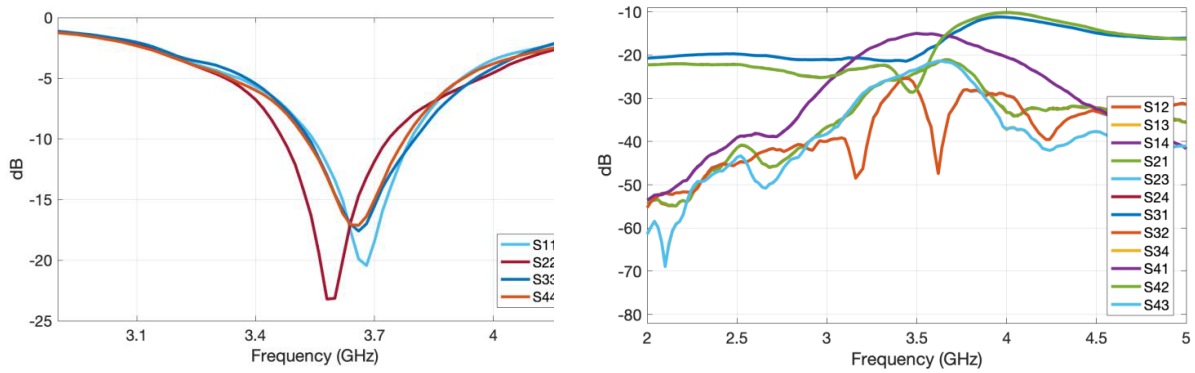

(a) (b)

Figure 14. The measured results of the reflection coefficients in (a) and the mutual coupling in (b) are for the first four MIMO antenna ports.

ports are also measured, as shown in Fig. 14(b), which are in good agreement with the simulation results, which were below almost −15 dB.

In order to assess the performance of the proposed 8×8 MIMO antenna, it is desirable to compare it with other state of the art mobile MIMO antenna designs from the literature. Table 2 presents a comparison of our proposed MIMO antenna with other MIMO antennas. The proposed MIMO antenna exhibits wideband impedance matching with high isolation between antenna elements more than 15 dB. Furthermore, the proposed MIMO design shows satisfactory far-field performance with computed maximum gain of 4.68 dB and efficiency of 90%. As for the MIMO performance metrics, the proposed design exhibits very low ECC as compared against many MIMO designs from the literature, where ECC below 0.01 was maintained over the 3.5 GHz band.

Table 2. Comparison of several existing MIMO antenna structures from literature with the proposed antenna prototype.

Reference	Antenna Type	Size (mm^2) (GHz)	Bandwidth Improvement (dB)	Isolation	Efficiency (%)	ECC
[22]	Coupled IFA	150×75	3.4–3.6	15	–	0.02
[23]	Inverted-F	100×50	3.4–3.6	10	55–60	–
[24]	Patch-Slot	150×75	3.5–3.6	11	52–76	–
[25]	Monopole	150×75	3.3–35	11	35–50	0.40
[33]	Spatial-Reuse Antenna	150×75	3.55–3.65	12	40–70	0.2
[34]	Inverted-L Monopole	136×68	3.4–3.6	14	40–60	0.2
[35]	Loop element	120×70	3.3–3.6	15	40	0.02
[36]	Wave-Guide	150×75	3.4–3.6	15	50–80	0.2
[37]	Monopole	136×68	4.5–4.7	10	50–70	–
[38]	Open-end slot	136×68	3.4–3.6	11	50–60	0.05
[39]	shorted-loop	150×77	3.4–3.6 GHz	10	78	< 0.055
This Work	**Hexagonal slots**	$\mathbf{150 \times 75}$	**3.35–3.8**	$\mathbf{> 15}$	**90–92**	$\mathbf{< 0.01}$

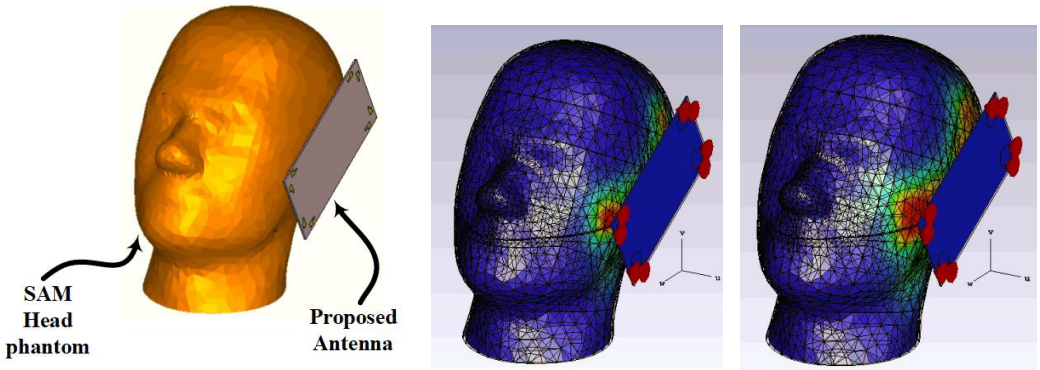

(a) (b) (c)

Figure 15. (a) Proposed antenna placed at distance off 5 mm away from SAM head phantom model. The SAR distribution inside the SAM head phantom model: (b) at 1 g and (c) 10 g were computed using the IEEE/IEC 62704-1 method. Note: that the color scale refers to a SAR values of 0 (dark blue color) and 0.95 (dark red color).

5. SPECIFIC ABSORPTION RATE (SAR)

A numerical simulation was conducted to investigate the distribution of the electromagnetic energy due to radiation from the proposed antenna using the specific absorption rate (SAR) inside the Standardized anthropomorphic (SAM) head phantom model. The SAR is defined as an amount of RF electromagnetic energy absorbed by biological tissue mass when it is exposed to radiating device at a certain frequency. It can be calculated as follows:

$$\mathrm{SAR} = \frac{\sigma |E|^2}{\rho} \tag{2}$$

where ρ is the mass density of the medium in (kg/m^3), σ the electrical conductivity in (S/m), and $|E|$ the magnitude of the electric field strength in (V/m). The proposed antenna is placed at a distance of 5 mm away from the SAM head phantom as shown in Fig. 15(a).

Figures 15(b) and (c) show the simulation result of the computed SAR distribution inside the SAM head phantom model at 1 g and 10 g using the IEEE/IEC 62704-1 method, where the peak values of SAR are 1.7 and 0.9 at 1 g and 10 g, respectively. The simulation results of SAR values at both mass tissues 1 g and 10 g demonstrate that these SAR values are approximately close to standard values of Federal Communication Commission (FCC).

6. CONCLUSION

A wideband polarization diversity MIMO antenna design is presented here for 5G smartphone terminals. The proposed MIMO array consists of eight L-shaped feeding ports with resonant octagon-shaped slots, which occupy only minimal spaces within the four corners of the printed circuit board that is also used for RF circuitries. Using octagon slot techniques, a wideband bandwidth with low mutual coupling between antenna' ports was achieved with satisfactory performance of far-field and MIMO metrics. Numerical full-wave simulation results agree very well with the fabricated and measured results. Based on the performance of the proposed 8×8 MIMO antenna structure, we believe that it is very promising for integration within 5G smart mobile handsets.

ACKNOWLEDGMENT

The authors extend their appreciation to the Deputyship for Research & Innovation, Ministry of Education in Saudi Arabia for funding this research work through the project number (IF-PSAU-2021/01/17697).

REFERENCES

1. Nadeem, Q.-U.-A., A. Kammoun, M. Debbah, et al., "Design of 5G full dimension massive MIMO systems," *IEEE Transactions on Communications*, Vol. 66, No. 2, 726–740, 2018.
2. Yang, H. and Y. Quek, *Massive MIMO Meet Small Cell: Backhaul and Cooperation*, SpringerBriefs in Electrical and Computer Engineering, Fort Lee, NJ, USA, 2017.
3. Osseiran, A., F. Boccardi, V. Braun, K. Kusume, P. Marsch, M. Maternia, O. Queseth, M. Schellmann, H. Schotten, H. Taoka, et al., "Scenarios for 5G mobile and wireless communications: The vision of the METIS project," *IEEE Communications Magazine*, Vol. 52, No. 5, 26–35, 2014.
4. Elshirkasi, A. M., A. A. Al-Hadi, R. Khan, P. Akkaraekthalin, H. S. B. Abdelmula, A. M. Belghasem, A. H. Jebril, and P. J. Soh, "Numerical analysis of users' body effects on a fourteen-element dual-band 5G MIMO mobile terminal antenna," *IEEE Access*, 2021.
5. Chang, L. and H. Wang, "Dual-band four-antenna module covering N78/N79 based on PIFA for 5G terminals," *IEEE Antennas and Wireless Propagation Letters*, Vol. 69, No. 9, 5297–5304, 2021.
6. Ye, Y., X. Zhao, and J. Wang, "Compact high-isolated MIMO antenna module with chip capacitive decoupler for 5G mobile terminals," *IEEE Antennas and Wireless Propagation Letters*, IEEE, 2022, doi: 10.1109/LAWP.2022.3152236.

7. Khan, J., S. Ullah, U. Ali, F. A. Tahir, I. Peter, and L. Matekovits, "Design of a millimeter-wave mimo antenna array for 5G communication terminals," *Sensors*, Vol. 22, No. 7, 2768, 2022.
8. Huang, H., W. Jiang, T. Zhang, Y. Zhu, B. Pang, and W. Hu, "Shared radiator based high-isolated tri-port mobile terminal antenna group design," *International Journal of RF and Microwave Computer-Aided Engineering*, e23177, 2022.
9. Abdullah, M., A. Altaf, M. R. Anjum, Z. A. Arain, A. A. Jamali, M. Alibakhshikenari, F. Falcone, and E. Limiti, "Future smartphone: MIMO antenna system for 5G mobile terminals," *IEEE Access*, Vol. 9, 91593–91603, 2021.
10. Hassan, N. and X. Fernando, "Massive MIMO wireless networks: An overview," *Electronics*, Vol. 6, No. 3, 63, 2017.
11. Pozar, D., "Analysis of finite phased arrays of printed dipoles," *IEEE Transactions on Antennas and Propagation*, Vol. 33, No. 10, 1045–1053, 1985.
12. Sharawi, M. S., "Printed multi-band mimo antenna systems and their performance metrics [wireless corner]," *IEEE Antennas and Propagation Magazine*, Vol. 55, No. 5, 218–232, 2013.
13. Mihaylov, G. Y., T. B. Iliev, T. D. Bikov, E. P. Ivanova, I. S. Stoyanov, V. P. Keseev, and A. R. Dinov, "Test cases and challenges for mobile network evolution from LTE to 5G," *2018 41st International Convention on Information and Communication Technology, Electronics and Microelectronics (MIPRO)*, 0449–0452, 2018.
14. Bait-Suwailam, M. M., O. Siddiqui, and O. Ramahi, "Mutual coupling reduction between microstrip patch antennas using slotted-complementary split-ring resonators," *IEEE Antennas and Wireless Propagation Letters*, Vol. 9, 876–878, 2010.
15. Sharawi, M. S., M. Ikram, and A. Shamim, "A two concentric slot loop based connected array MIMO antenna system for 4G/5G terminals," *IEEE Transactions on Antennas and Propagation*, Vol. 65, No. 12, 6679–6686, 2017.
16. Al Abbas, E., M. Ikram, A. T. Mobashsher, and A. Abbosh, "MIMO antenna system for multi-band millimeter-wave 5G and wideband 4G mobile communications," *IEEE Access*, Vol. 7, 181916–181923, 2019.
17. Liu, Y., Z. Ai, G. Liu, and Y. Jia, "An integrated shark-fin antenna for MIMO-LTE, FM, and GPS applications," *IEEE Antennas and Wireless Propagation Letters*, Vol. 18, No. 8, 1666–1670, 2019.
18. Cihangir, A., F. Ferrero, G. Jacquemod, P. Brachat, and C. Luxey, "Neutralized coupling elements for MIMO operation in 4G mobile terminals," *IEEE Antennas and Wireless Propagation Letters*, Vol. 13, 141–144, 2014.
19. Wang, Y. and Z. Du, "A printed dual-antenna system operating in the GSM1800/GSM1900/UMTS/LTE2300/LTE2500/2.4-GHz WLAN bands for mobile terminals," *IEEE Antennas and Wireless Propagation Letters*, Vol. 13, 233–236, 2014.
20. Larsson, E. G., O. Edfors, F. Tufvesson, and T. L. Marzetta, "Massive MIMO for next generation wireless systems," *IEEE Communications Magazine*, Vol. 52, No. 2, 186–195, 2014.
21. Al-Hadi, A., J. Ilvonen, R. Valkonen, and V. Viikan, "Eight-element antenna array for diversity and MIMO mobile terminal in LTE 3500 MHz band," *Microwave and Optical Technology Letters*, Vol. 56, 1323–1327, 2014.
22. Liu, Y., Y. Lu, Y. Zhang, and S.-X. Gong, "MIMO antenna array for 5G smartphone applications," *2019 13th European Conference on Antennas and Propagation (EuCAP)*, 1–3, IEEE, 2019.
23. Al-Hadi, A. A., J. Ilvonen, R. Valkonen, and V. Viikari, "Eight-element antenna array for diversity and MIMO mobile terminal in LTE 3500 MHz band," *Microwave and Optical Technology Letters*, Vol. 56, No. 6, 1323–1327, 2014.
24. Parchin, N. O., Y. I. Al-Yasir, J. M. Noras, and R. A. Abd-Alhameed, "Dual-polarized mimo antenna array design using miniaturized self-complementary structures for 5G smartphone applications," *2019 13th European Conference on Antennas and Propagation (EuCAP)*, 1–4, IEEE, Krakow, Poland, 2019.

25. Wong, K.-L., J.-Y. Lu, L.-Y. Chen, W.-Y. Li, and Y.-L. Ban, "8-antenna and 16-antenna arrays using the quad-antenna linear array as a building block for the 3.5-GHz LTE MIMO operation in the smartphone," *Microwave and Optical Technology Letters*, Vol. 58, No. 1, 174–181, 2016.
26. Chen, Q., H. Lin, J. Wang, L. Ge, Y. Li, T. Pei, et al., "Single ring slot-based antennas for metal-rimmed 4G/5G smartphones," *IEEE Transactions on Antennas and Propagation*, Vol. 67, No. 3, 1476–1487, 2018.
27. Habaebi, M. H., M. Janat, and M. R. Islam, "Beam steering antenna array for 5G telecommunication systems applications," *Progress In Electromagnetics Research M*, Vol. 67, 197–207, 2018.
28. Parchin, N. O., Y. Al-Yasir, A. M. Abdulkhaleq, I. Elfergani, A. Rayit, J. M. Noras, J. Rodriguez, and R. A. Abd-Alhameed, "Frequency reconfigurable antenna array for mm-Wave 5G mobile handsets," *Proceedings of the 9th International Conference on Broadband Communications, Networks, and Systems*, 438–445, Springer, Faro, Portugal, 2018.
29. Bjornson, E., L. van der Perre, S. Buzzi, and E. G. Larsson, "Massive MIMO in sub-6 GHz and mmwave: Physical, practical, and use-case differences," *IEEE Wireless Communications*, Vol. 26, No. 2, 100–108, 2019.
30. Al-Yasir, Y. I., A. S. Abdullah, N. Ojaroudi Parchin, R. A. Abd-Alhameed, and J. M. Noras, "A new polarization-reconfigurable antenna for 5G applications," *Electronics*, Vol. 7, No. 11, 293, 2018.
31. Hussain, R., A. T. Alreshaid, S. K. Podilchak, and M. S. Sharawi, "Compact 4G MIMO antenna integrated with a 5G array for current and future mobile handsets," *IET Microwaves, Antennas & Propagation*, Vol. 11, No. 2, 271–279, 2017.
32. Blanch, S., J. Romeu, and I. Corbella, "Exact representation of antenna system diversity performance from input parameter description," *Electronics Letters*, Vol. 39, No. 9, 705–707, May 2003.
33. Chang, L., Y. Yu, K. Wei, and H. Wang, "Polarization-orthogonal co-frequency dual antenna pair suitable for 5G MIMO smartphone with metallic bezels," *IEEE Transactions on Antennas and Propagation*, Vol. 67, No. 8, 5212–5220, 2019.
34. Abdullah, M., Y.-L. Ban, K. Kang, M.-Y. Li, and M. Amin, "Eight-element antenna array at 3.5 GHz for MIMO wireless application," *Progress In Electromagnetics Research C*, Vol. 78, 209–216, 2017.
35. Jiang, W., B. Liu, Y. Cui, and W. Hu, "High-isolation eight-element MIMO array for 5G smartphone applications," *IEEE Access*, Vol. 7, 34104–34112, 2019.
36. Li, M.-Y., Y.-L. Ban, Z.-Q. Xu, J. Guo, and Z.-F. Yu, "Tri-polarized 12-antenna MIMO array for future 5G smartphone applications," *IEEE Access*, Vol. 6, 6160–6170, 2017.
37. Xu, S., M. Zhang, H. Wen, and J. Wang, "Deep-subwavelength decoupling for MIMO antennas in mobile handsets with singular medium," *Scientific Reports*, Vol. 7, 12162, 2017.
38. Abdullah, M., S. H. Kiani, L. F. Abdulrazak, A. Iqbal, M. Bashir, S. Khan, and S. Kim, "High-performance multiple-input multiple-output antenna system for 5G mobile terminals," *Electronics*, Vol. 8, No. 1090, 1–16, 2019.
39. Alja'afreh, S. S., B. Altarawneh, M. H. Alshamaileh, E. R. Almajali, R. Hussain, M. S. Sharawi, L. Xing, and Q. Xu, "Ten antenna array using a small footprint capacitive-coupled-shorted loop antenna for 3.5 GHz 5G smartphone applications," *IEEE Access*, Vol. 9, 33796–33810, 2021.